PHYSICAL REVIEW A

ATOMIC, MOLECULAR, AND OPTICAL PHYSICS

THIRD SERIES, VOLUME 59, NUMBER 6 JUNE 1999

RAPID COMMUNICATIONS

The Rapid Communications section is intended for the accelerated publication of important new results. Since manuscripts submitted to this section are given priority treatment both in the editorial office and in production, authors should explain in their submittal letter why the work justifies this special handling. A Rapid Communication should be no longer than 4 printed pages and must be accompanied by an abstract. Page proofs are sent to authors.

Role of exchange and kinematic in the generation of low-energy polarized electron pairs

M. Streun,[1] G. Baum,[1] W. Blask,[1] and J. Berakdar[2]
[1]*Fakultät für Physik, Universität Bielefeld, 33615 Bielefeld, Germany*
[2]*Max-Planck Institut für Mikrostrukturphysik, Weinberg 2, 06120 Halle, Germany*
(Received 28 January 1999)

Spin-polarized electron pairs are generated following the ionization of the valence electron of polarized Li atoms by polarized low-energy electron impact. It is shown that the shapes of energy-sharing spectra of the pairs are influenced by an interplay of structures resulting from binary-encounter and exchange effects of the two electrons. The spin asymmetry is measured at an excess energy as low as 20 eV and compared with dynamical calculations of different models. The shape of the asymmetry is explained on the grounds of symmetry and dynamics. [S1050-2947(99)50106-6]

PACS number(s): 34.80.Nz

Spin-dependent effects in electron (ionizing) collisions can be traced back to exchange and/or spin-orbit interactions. Spin-orbit effects are prominant when the spins of the electrons are strongly coupled to the electrons' angular momenta [1,2]. Such effects of the spin-orbit coupling can be observed in the single ionization of the *K*- and *L*-shell electrons of heavy-metal targets upon the impact of spin-polarized electrons [3–6]. On the other hand, exchange interaction is a consequence of the fermionic nature of the electrons that imposes the Pauli principle on the wave function. In an electron-impact ionizing reaction with spin-polarized partners the strength of the exchange interaction between the two escaping electrons can be studied [7,8]. It is very much dependent on the collision geometry, but is present for all atomic targets, whereas spin-orbit effects diminish with decreasing strength of the Coulomb nuclear field, i.e., for light targets [1]. Effects arising from spin-orbit and exchange coupling may also interfere, as is the case in the incidence of polarized electrons on a heavy target while the fine structure of the final ion state is resolved [9–16].

In a spin nonresolved electron-impact ionization process the electrons' spectra are deduced as a statistical average of the individual spin channels. However, structures of the individual spin contributions may still be observable in the spin nonresolved cross sections. Such a case has recently been pointed out in Ref. [17]. There, certain structures in the spin nonresolved angular distribution of electrons emitted upon electron impact on $H(1s)$ and $He(^1S^e)$ have been attributed to an interplay between exchange effects and the effects of binary collisions (see also [18], and references therein). This conclusion has been inferred from the analysis of the contributing spin-resolved cross sections.

Our experimental and theoretical work aims at the explicit investigation of the spin-resolved cross sections at low energies. This yields a direct insight into the interplay between kinematic and exchange effects. To this end we consider the ionization of the valence electron of polarized Li atoms by polarized electron impact. The two escaping electrons in the final channel are detected in coincidence. Their energies E_a, E_b are resolved using two electrostatic hemispherical spectrometers positioned in a plane that contains the incident electron beam. For fixed angular positions of the spectrometers with angles of $\Delta\Theta_a = -\Delta\Theta_b = 45°$, where the two electrons escape perpendicular to each other, and for fixed excess energy $E := E_a + E_b$ ($E = 20$ eV in the present measurements), we study the dependence of the count rates on the energy sharing $\alpha = (E_a - E_b)/E$. The apparatus is described in more detail elsewhere [8].

The spin asymmetry A provides information about the spin dependence of the triple differential cross section σ. It is defined as the relative difference between the cross sections for antiparallel and parallel spin combinations of the colliding particles:

$$A=\frac{\sigma^{\uparrow\downarrow}-\sigma^{\uparrow\uparrow}}{\sigma^{\uparrow\downarrow}+\sigma^{\uparrow\uparrow}}. \tag{1}$$

From the observed number of coincident-electron counts $N^{\uparrow\downarrow/\uparrow\uparrow}$ for each spin combination we obtain the ''raw'' asymmetry

$$A^{\mathrm{raw}}=\frac{N^{\uparrow\downarrow}-N^{\uparrow\uparrow}}{N^{\uparrow\downarrow}+N^{\uparrow\uparrow}}=|\mathbf{P}_a\cdot\mathbf{P}_e|A, \tag{2}$$

which we relate to A by taking the nonperfect beam polarizations $(\mathbf{P}_a,\mathbf{P}_b)$ into account as indicated in Eq. (2). During the measurements, the spin settings of the Li beam as well as those of the electron beam were alternated in short time intervals to reduce systematic errors.

The ions produced in the scattering region represent a measure of the total ionization cross section. They are exploited for determining the product of the beam polarizations, $|\mathbf{P}_a\cdot\mathbf{P}_e|$. To this purpose, we record ion counts concurrently with the electron coincidences and obtain, in an analogous way to Eq. (2), the ''raw'' spin asymmetry of the total ionization, $A_{\mathrm{ion}}^{\mathrm{raw}}$. The physical spin asymmetry A_{ion}, of the total ionization is known experimentally [19], as well as theoretically [20,21], with good agreement between the two. Thus we obtain the spin asymmetry A of Eq. (1) from

$$A=\frac{A_{\mathrm{ion}}}{A_{\mathrm{ion}}^{\mathrm{raw}}}A^{\mathrm{raw}}. \tag{3}$$

Normalizing in this way is more direct and carries smaller systematic uncertainties than using the individual beam polarizations, as measured separately with respective polarimeters.

The energy and angular acceptances of each electron detection system depend on the electron-optical setting of the lens system in front of the hemispherical electrostatic spectrometer. The coincidence energy acceptance ΔE_{ab} can be obtained from

$$\Delta E_{ab}^{-2}=\Delta E_a^{-2}+\Delta E_b^{-2}, \tag{4}$$

where $\Delta E_a,\Delta E_b$ are the single acceptances of the electron detectors [22]. In our measurement ($E=20$ eV) the energy sharing varies between $\alpha=-0.8$ for an extremly asymmetric case and $\alpha=0.2$ for a measurement going beyond the symmetric case where $E_a=E_b$. Hence, the energy of one of the electrons E_a varies between 2 and 12 eV (thus, $E_b\in[8,18\ \mathrm{eV}]$). As the accepted energy width depends on the pass energy of the electrons through the analyzer, we choose for the typically slow electron of detector a an acceleration factor of 5 in the lens system, giving a correspondingly increased pass energy, and for the typically fast electron of detector b an acceleration factor of 1, as was done in our previous investigations [8]. In this way the energy acceptance is increased for the ''slow'' detector and, in addition, the coincidence energy acceptance of Eq. (4) is almost equal for each data point from $E_a=2$ eV to $E_a=12$ eV. As an effect of the different settings for the optics, the two detectors have different angular acceptances with full width at half maximum values of $\Delta\Theta_a=20°$ and $\Delta\Theta_b=10°$. The spin asymmetry must be symmetric to the $E_a=10$ eV line; that is, the asymmetries for $E_a=8$ eV and $E_a=12$ eV should be identical. However, besides statistical fluctuations, the different experimental conditions for these two settings, especially for the angular acceptance, may lead to small deviations from this expectation.

For light targets such as Li we can neglect spin-orbit interaction. Thus, the spin asymmetry is primarily due to exchange and can be expressed in terms of the singlet and triplet scattering cross sections σ_s and σ_t, respectively:

$$A=\frac{\sigma_s-\sigma_t}{\sigma_s+3\sigma_t}. \tag{5}$$

The singlet and triplet scattering cross sections are obtained from the corresponding transition matrix elements T_s and T_t via the relation

$$\sigma_{s/t}(E_a,E_b,\Omega_a,\Omega_b)=(2\pi)^4\frac{k_ak_b}{k_i}|T_{s/t}|^2, \tag{6}$$

where $\mathbf{k}_i$, $\mathbf{k}_b$, and $\mathbf{k}_a$ are the momenta of the incoming electrons and the two emitted electrons, respectively, and Ω_a,Ω_b are the solid angles associated with $\mathbf{k}_a$ and $\mathbf{k}_b$ with respect to the incident direction. The matrix elements $T_{s/t}$ represent the transition operators $\mathcal{T}_{s/t}$ where

$$\mathcal{T}_s=(I+\mathcal{P}_{ab})\mathcal{T}_{fi}(\mathbf{k}_a,\mathbf{k}_b),\quad \mathcal{T}_t=(I-\mathcal{P}_{ab})\mathcal{T}_{fi}(\mathbf{k}_a,\mathbf{k}_b). \tag{7}$$

The action of the exchange operator $\mathcal{P}_{ab}$ on $\mathcal{T}_{fi}$ is given by $\mathcal{P}_{ab}\mathcal{T}_{fi}(\mathbf{k}_a,\mathbf{k}_b)=\mathcal{T}_{fi}(\mathbf{k}_b,\mathbf{k}_a)$. The operator $\mathcal{T}_{fi}$ is represented by the matrix element

$$T_{fi}(\mathbf{k}_a,\mathbf{k}_b)=\langle\Psi|V_i|\phi,\mathbf{k}_i\rangle. \tag{8}$$

Here we assume $|\phi,\mathbf{k}_i\rangle$ to be the asymptotic initial state consisting of a product of an incoming plane wave describing the incident projectile and a single-particle $2s$ Hartree orbital of Li [23]. The perturbation operator V_i occurring in Eq. (8) is the Coulomb scattering potential from the active valence electron of Li and from the core (Li^+).

The state vector $\langle\Psi|$ in Eq. (8) describes the two-continuum electrons' motion in the field of Li^+. Two approximate expressions are used to represent $\langle\Psi|$: the 3C model [24] in which the three-body system (two electrons and the Li^+ core) is broken down into three noninteracting two-body subsystems, and the DS3C approach that accounts for dynamical screening within each of the two-body interacting Coulomb subsystems [25,26]. Both of these models have been extensively studied (see [26], and references therein) and their mathematical details are not repeated here.

To exhibit the competition between collisional ionization processes, i.e., effects due to binary encounter between the collision partners, and exchange effects, we focus on the following geometry. The escaping electrons are detected, coplanar with $\mathbf{k}_i$, under an angle of 45° with respect to $\mathbf{k}_i$ and perpendicular to each other; i.e., $(\hat{\mathbf{k}}_a\times\hat{\mathbf{k}}_b)\cdot\hat{\mathbf{k}}_i=0,\hat{\mathbf{k}}_a\cdot\hat{\mathbf{k}}_b=0,\hat{\mathbf{k}}_a\cdot\hat{\mathbf{k}}_i=\cos\pi/4=\hat{\mathbf{k}}_b\cdot\hat{\mathbf{k}}_i$ [see inset in Fig. 1(c)].

For a fixed excess energy, $E=20$ eV, the asymmetry A is scanned as function of the energy sharing $(E_a-E_b)/E=:\alpha\in[-1,1]$. For $\alpha=0(E_a=E_b)$ we arrive at the condition for

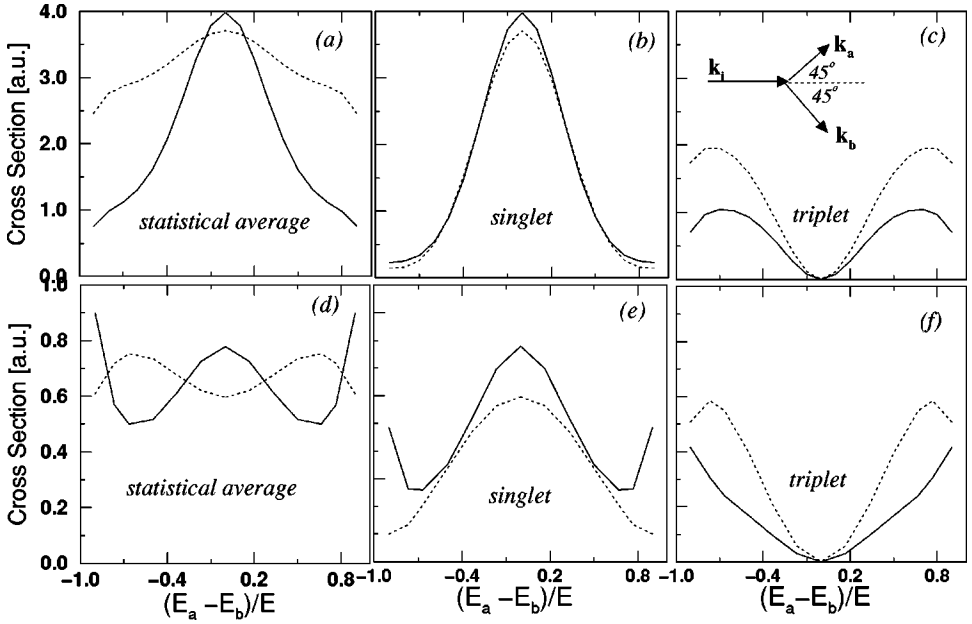

FIG. 1. (a) Spin nonresolved cross section for the electron-impact ionization of the valence electron of Li as a function of the energy sharing $(E_a-E_b)/E$, where E_a and E_b are the energies of the continuum electrons. The calculations have been performed with the 3C model (dotted curve) and the DS3C theory (solid curve). The corresponding singlet and triplet cross sections are depicted in (b) and (c), respectively. All 3C cross sections have been multiplied by a factor of 4. The total kinetic energy of the escaping electrons is $E=20$ eV. Both electrons are detected coplanar with the incident direction $\mathbf{k}_i$. The electrons escape perpendicular to each other, whereby $\mathbf{k}_i$ bisects the interelectronic relative angle [see inset in (c)]. (d)–(f) Same as in (a)–(c), with the same notation; however, the excess energy is lowered to $E=6$ eV. The 3C results have been multiplied by a factor of 20.

a direct (classical) encounter of the incoming projectile with a stationary valence electron. Therefore, in the singlet cross section σ_s [Fig. 1(b)], a pronounced peak arises at $\alpha=0$. On the other hand, due to the cylindrical symmetry of the whole

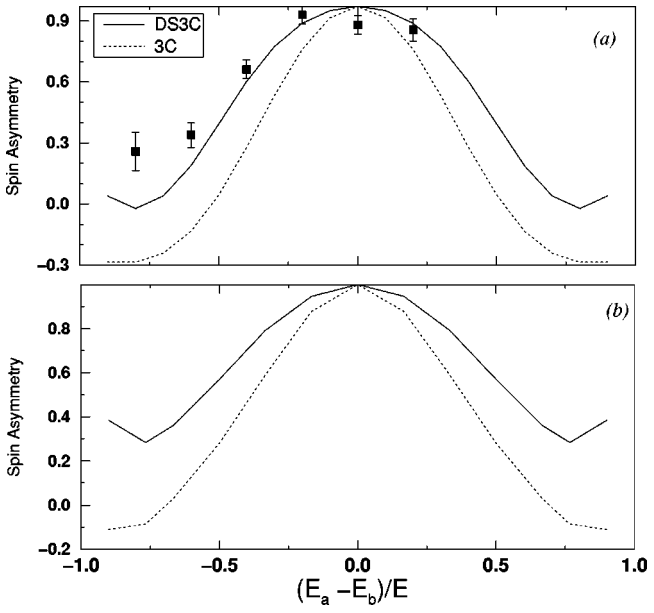

FIG. 2. (a) Spin asymmetry corresponding to the situation of Figs. 1(a)–1(c). The 3C (dotted curve) and DS3C (solid curve) results are shown along with the experimental findings (full squares). Theoretical results have not been convoluted by the finite experimental resolution. In (b) the spin asymmetry associated with the geometry of Figs. 1(d)–1(f) is shown; 3C (dotted) and DS3C (solid curve) calculations are depicted.

experiment with respect to $\hat{\mathbf{k}}_i$, the triplet scattering cross section σ_t vanishes at $\alpha=0$ $(E_a=E_b)$ [Fig. 1(c)]. The shape of the spin-averaged cross section, $\sigma=0.25\sigma_s+0.75\sigma_t$ [cf. Fig. 1(a)], is now very much dependent on the ratio of the singlet [Fig. 1(b)] to the triplet [Fig. 1(c)] cross section and hence on the spin asymmetry. Dominant triplet scattering leads to a decreased spin nonresolved cross section at $\alpha=0$ (due to the zero point in σ_t at $\alpha=0$ that results from exchange) [cf. the 3C results in Fig. 1(d)], whereas a dominant singlet scattering yields a maximum at $\alpha=0$ in the cross section (due to the peak in σ_s at $\alpha=0$ that originates from the direct electron-electron encounter), as observed in Fig. 1(a). Generally the ratio of singlet-to-triplet cross sections, which is closely related to A, is a dynamical quantity that depends sensitively on the dynamical model used to describe the collision process, as demonstrated below.

The spin asymmetry A [Eq. (1)] for the geometry of Fig. 2(a) reveals a smooth decrease away from $\alpha=0$ where it should be unity ($\sigma_t=0$ at $\alpha=0$). The DS3C calculations are in good agreement with the experimental data, whereas the predictions of the 3C model deviate considerably from the measured asymmetry values. This is consistent with the finding of a previous study on the spin asymmetry in integrated cross sections [27,28]. There, the 3C model systematically underestimated the value of A, whereas the DS3C theory performed satisfactorily. Since the difference between the DS3C and the 3C treatment is the neglect of three-body coupling in the 3C model, we can conclude that the spin asymmetry is influenced considerably by the three-body dynamics.

At higher energies and small momentum transfer [$E\gg1$ and one electron is very slow ($\alpha=\pm1$)] the ionization pro-

cess is dominated by direct scattering [29]. To see how this is being reflected into the spin asymmetry, we write A in the form $A=|f|\ |g|\cos\delta/(|f|^2+|g|^2+|f-g|^2)$ [30], where f and g are, respectively, the direct and exchange scattering amplitudes and δ is their relative phase. Thus, for $E\gg 1$ and $\alpha=\pm 1$ the spin asymmetry diminishes as $\lim_{E\gg 1,\alpha=\pm 1}A \rightarrow |g|/|f|\rightarrow 0$ (in this limit $|f|\gg|g|$ [29]). Similarly, $\lim_{|g|\gg|f|}A\rightarrow|f|/|g|\rightarrow 0$, i.e., A is of a sizable magnitude only when $|f|$ and $|g|$ are of the same order.

A reminiscence of this behavior is observed in Fig. 2(a). The asymmetry decreases drastically for $\alpha\rightarrow\pm 1$. Going down with the excess energy [Fig. 2(b)], the asymmetry A should increase for $\alpha=\pm 1$ as the exchange amplitude $|g|$ enhances (as compared to $|f|$). The DS3C results confirm this behavior [cf. Fig. 2(b)].

At low excess energy ($E=6$ eV) [Figs. 1(d)–1(f)] we notice a drastically different behavior as compared to the $E=20$ eV case. The triplet (singlet) cross section still shows a zero (peak) at $\alpha=0$ for the reasons mentioned above. However, the ratio of the magnitude of σ_s to that of σ_t changes (σ_t becomes more pronounced). As a consequence, the 3C spin-averaged cross section [Fig. 1(d)] reveals a minimum at $\alpha=0$. In contrast, the DS3C model predicts a dominant singlet scattering. Therefore, the DS3C results for σ show a maximum at $\alpha=0$ that stems from σ_s. However, this peak in σ is less pronounced than the corresponding one in σ_s due to vanishing contribution from σ_t at $\alpha=0$. At even lower energies the DS3C anticipates an enhanced triplet cross section and hence the spin-averaged cross section also reveals a minimum at $\alpha=0$.

The rough structure of the cross sections in Figs. 1 and 2 can be explained qualitatively by assuming that the cross sections should reveal a maximum around $\alpha=0$ for kinematical reasons (at $\alpha=0$ the condition for direct binary encounter is fulfilled). Now combining this form with the Pauli minimum at $\alpha=0$ we end up with the shape of σ_t as depicted in Figs. 1(c) and 1(f). For example, in Fig. 1(c) σ_t possesses a maximum at $\alpha=\pm 0.75$. The origin of this maximum is basically the minimum at $\alpha=0$, i.e., σ_t rises when α varies from $\alpha=-1$ to $\alpha=0$ in the same way σ_s does. Due to the Pauli minimum at $\alpha=0$, however, σ_t drops to zero at $\alpha=0$, leaving the ''hills'' around $\alpha=\pm 0.75$. The same analysis applies to Fig. 1(f).

Comparing Fig. 2 and Fig. 1 it is obvious that, in addition to the spin asymmetry, a measurement of the spin nonresolved cross sections or the singlet and triplet cross sections is indispensible to arrive at unambiguous information on the precise contribution of kinematical versus exchange effects. Unfortunately, none of those measurements are available yet and an experimental endeavor in this direction is most desirable.

[1] J. Kessler, *Polarized Electrons* (Springer-Verlag, Berlin, 1976).
[2] J. Kirschner, *Polarized Electrons at Surfaces* (Springer-Verlag, Berlin, 1985).
[3] H.-Th. Prinz, K.-H. Besch, and W. Nakel, Phys. Rev. Lett. **74**, 243 (1995).
[4] M. Sauter, H. Ott, and W. Nakel, J. Phys. B **31**, L967 (1998).
[5] S. Keller, C.T. Whelan, H. Ast, H.R.J. Walters, and R.M. Dreizler, Phys. Rev. A **50**, 3865 (1994).
[6] S. Keller, R.M. Dreizler, L.U. Ancarani, H. Ast, H.R.J. Walters, and C.T. Whelan (unpublished).
[7] G. Baum, W. Blask, P. Freienstein, L. Frost, S. Hesse, W. Raith, P. Rappolt, and M. Streun, Phys. Rev. Lett. **69**, 3037 (1992).
[8] M. Streun, G. Baum, W. Blask, J. Rasch, I. Bray, D.V. Fursa, S. Jones, D.H. Madison, H.R.J. Walters, and C.T. Whelan, J. Phys. B **31**, 4401 (1998).
[9] G.F. Hanne, Can. J. Phys. **74**, 811 (1996).
[10] B. Granitza, X. Guo, J.M. Hurn, J. Lower, S. Mazevet, I.E. McCarthy, Y. Shen, and E. Weigold, Aust. J. Phys. **49**, 383 (1996).
[11] A. Dorn, A. Elliot, X. Guo, J. Hurn, J. Lower, S. Mazevet, I.E. McCarthy, Y. Shen, and E. Weigold, J. Phys. B **30**, 4097 (1997).
[12] C. Mette, T. Simon, C. Herting, G.F. Hanne, and D.H. Madison, J. Phys. B **31**, 4689 (1998).
[13] K.-H. Besch, M. Sauter, and W. Nakel, Phys. Rev. A **58**, R2638 (1998).
[14] S. Keller, R.M. Dreizler, H. Ast, C.T. Whelan, and H.R.J. Walters, Phys. Rev. A **53**, 2295 (1996).
[15] S. Mazevet, Ph.D. thesis, Australian National University, 1997 (unpublished).
[16] D.H. Madison, V.D. Kravtsov, and S. Mazevet, J. Phys. B **31**, L17 (1998).
[17] J. Berakdar and J.S. Briggs, J. Phys. B **29**, 2289 (1996).
[18] J. Berakdar, J. S. Briggs, I. Bray, and D. V. Fursa, J. Phys. B **32**, 895 (1999).
[19] G. Baum, M. Moede, W. Raith, and W. Schröder, J. Phys. B **18**, 531 (1985).
[20] I. Bray, D.V. Fursa, and I.E. McCarthy, Phys. Rev. A **47**, 1101 (1993).
[21] I. Bray, J. Phys. B **28**, L247 (1995).
[22] A. Lahmam-Bennani, H.F. Wellenstein, A. Duguet, and M. Lecas, Rev. Sci. Instrum. **56**, 43 (1985).
[23] T. Inui and Y. Uemura, Prog. Theor. Phys. (Kyoto) **56**, 252 (1950).
[24] M. Brauner, J.S. Briggs, and H. Klar, J. Phys. B **22**, 2265 (1989).
[25] J. Berakdar, Phys. Rev. A **53**, 2314 (1996).
[26] J. Berakdar, Phys. Rev. A **56**, 370 (1997).
[27] J. Berakdar, Aust. J. Phys. **49**, 1095 (1996).
[28] J. Berakdar, P.F. O'Mahony, and F. Mota-Furtado, Z. Phys. D **39**, 41 (1997).
[29] C.J. Joachain, Comments At. Mol. Phys. **17**, 261 (1986).
[30] J. Berakdar and J.S. Buckman, Phys. Rev. A **54**, 5431 (1996).